

An electronic band sculpted by oxygen vacancies and indispensable for dilute superconductivity

Benoît Fauqué¹, Clément Collignon^{1,2,*}, Hyeok Yoon^{3,4,†}, Ravi², Xiao

Lin^{2,‡}, Igor I. Mazin⁵, Harold Y. Hwang^{3,4}, and Kamran Behnia²

(1) JEIP (USR 3573 CNRS), Collège de France, 75005 Paris, France

(2) Laboratoire de Physique et d'Etude de Matériaux (CNRS)

ESPCI Paris, Université PSL, 75005 Paris, France

(3) Stanford Institute for Materials and Energy Sciences,

SLAC National Accelerator Laboratory, Menlo Park, Stanford, California 94025, USA

(4) Department of Applied Physics, Stanford University, Stanford, California 94305, USA

(5) Department of Physics and Astronomy and Quantum Science and Engineering Center,
George Mason University, Fairfax, Virginia 22030, USA

(Dated: August 23, 2022)

Dilute superconductivity survives in bulk strontium titanate when the Fermi temperature falls well below the Debye temperature. Here, we show that the onset of the superconducting dome is dopant-dependent. When mobile electrons are introduced by removing oxygen atoms, the superconducting transition survives down to $2 \times 10^{17} \text{ cm}^{-3}$, but when they are brought by substituting Nb with Ti, the threshold density for superconductivity is an order of magnitude higher. Our study of quantum oscillations reveals a significant difference in the band dispersion between the dilute metals made by these doping routes and our band calculations demonstrate that the rigid band approximation does not hold when mobile electrons are introduced by oxygen vacancies. We identify the band sculpted by these vacancies as the exclusive locus of superconducting instability in the ultra-dilute limit.

Discovered half a century ago [1], superconductivity in strontium titanate is attracting renewed attention [2, 3]. It lies beyond the Migdal-Eliashberg [4] framework, since the Fermi temperature of electrons falls below the Debye temperature of phonons [5, 6]. The dilute metal going through this superconducting instability has non-trivial transport properties [7–10]. The insulating parent, identified as a quantum paraelectric [11], due to its huge permittivity, displays an unusual low-temperature thermal conductivity [12] and a puzzling thermal Hall effect [13]. Soft transverse optical phonons, hybridizing with transverse acoustic phonons at low temperatures [14, 15], are suspected to play a major role in this solid.

The proximity to a ferroelectric instability is often invoked in explaining superconductivity [16–18]. Several experimental studies have documented a constructive interplay between superconductivity and ferroelectricity [19–22] and recent theoretical accounts of Cooper pairing invoke the exchange of two [23–25] or one [26, 27] soft phonons between pairing electrons. A two-phonon exchange scenario, first invoked decades ago [28], leads to instantaneous electron-electron attraction and can explain [24] the experimentally-observed persistence of superconductivity at densities below 10^{18} cm^{-3} [5, 29].

Here, we present a study of superconducting transition and quantum oscillations in oxygen-reduced and Nb-substituted strontium titanate in the dilute limit. We

find that when $n < 5 \times 10^{18} \text{ cm}^{-3}$, superconductivity is present in $\text{SrTiO}_{3-\delta}$, but absent in $\text{SrTi}_{1-x}\text{Nb}_x\text{O}_3$, either single-crystalline or custom-made thin films. The dilute metals generated by these alternative doping routes are also different. Compared to $\text{SrTiO}_{3-\delta}$, $\text{SrTi}_{1-x}\text{Nb}_x\text{O}_3$ has a less spherical Fermi surface and hosts lighter electrons. Moreover, the Lifshitz transition occurs at a lower density. We present numerical evidence that the virtual crystal approximation used in the LDA band calculations [30] holds for Nb doping, but not for oxygen deficiency. We conclude that while both doping routes generate a superconducting ground state, dilute superconductivity (arising in a metal where e-e distance of the order 10 nm) occurs only when the occupied band is sculpted by oxygen vacancies. A larger coupling between the electrons of the vacancy-sculpted band and soft TO phonons, or a larger electronic density of states, or a combination of both, may be the origin.

SrTiO_3 can be n-doped by a variety of atomic substitutions. The focus of the present study is to compare substitution of tetravalent Ti^{4+} by pentavalent Nb^{5+} with creation of oxygen vacancies. While both lead to n-doping, there is no *a priori* reason to believe that they affect the electronic structure in the same way [32]. In presence of an O vacancy, the two neighboring Ti ions are left with one extra electron each. What can happen with these electrons? They can either get collectively extended over all Ti sites or both occupy the vacancy. In a recent DFT+DMFT calculation, Souto-Casares, Spaldin and Ederer [33] found that if the Hubbard repulsion on Ti and the concentration are both large, one or even two electrons will prefer to avoid the Hubbard repulsion on Ti and “hide” in the vacancy. However, the effective concentration of vacancies in that work [33] was one

* Present address: Department of Physics, Massachusetts Institute of Technology, Cambridge, Massachusetts 02139, USA

† Present address: Department of Physics, University of Maryland, College Park, Maryland 20742, USA

‡ Present address: School of Science, Westlake University, 18 Shilongshan Road, 310024 Hangzhou, China

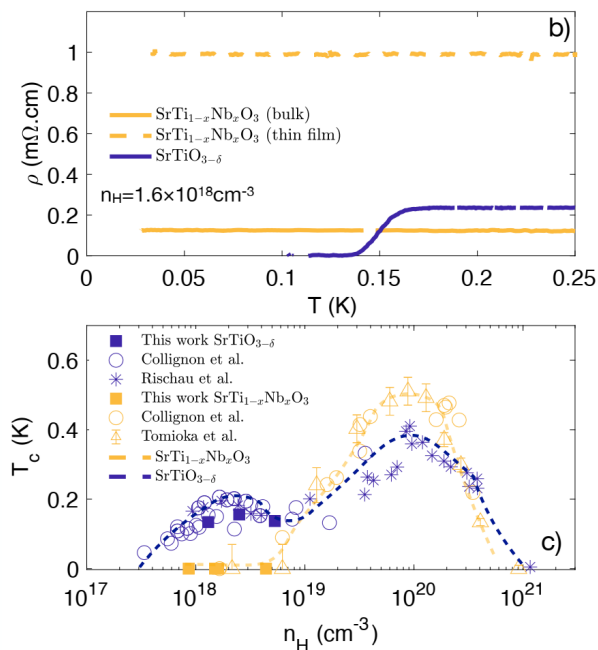


FIG. 1. **Different thresholds for emergence of superconductivity:** a) Temperature dependence of electrical resistivity (ρ_{xx}) in SrTi_{1-x}Nb_xO₃ and SrTiO_{3- δ} (orange) sample with similar carrier density $n_H \simeq 1.6 \times 10^{18} \text{cm}^{-3}$. Neither the thin film nor the single crystalline SrTi_{1-x}Nb_xO₃ shows a superconducting transition at this carrier density. b) Doping evolution of the superconducting critical temperature (T_c). Solid symbols represent samples studied in the present work. Open symbols represent what was reported previously [2, 22, 31].

per four formula units, which is several orders of magnitude higher than the relevant experimental range. At very small concentrations, Hubbard correlation between the doped electrons, included in the DMFT method and not in the DFT, are much less important than geometric changes such as lattice relaxation. Keeping this in mind, we have performed full structural relaxation in the density functional theory (DFT), using an $8 \times 8 \times 8$ supercell of 64 f.u., and either replacing one Ti with Nb or removing one O. As discussed below, we found that the resulting electronic structure near the bottom of the conduction band is dramatically different in the two cases.

Fig.1a shows the low-temperature electrical resistivity (ρ_{xx}) of three samples with the same Hall carrier density. One can see that SrTiO_{3- δ} becomes a superconductor, but not SrTi_{1-x}Nb_xTiO₃ (at least not down to 30mK). Note that, the oxygen deficient sample has a residual resistivity lower than the thin film and larger than the crystalline SrTi_{1-x}Nb_xTiO₃. This rules out disorder as the driver of this dichotomy. Studying four different Nb-doped SrTiO₃ thin films [34] with a thickness of ≈ 900 nm and nominal Nb concentrations of 0.02 and 0.04 atomic percent, we found that none was superconducting (See

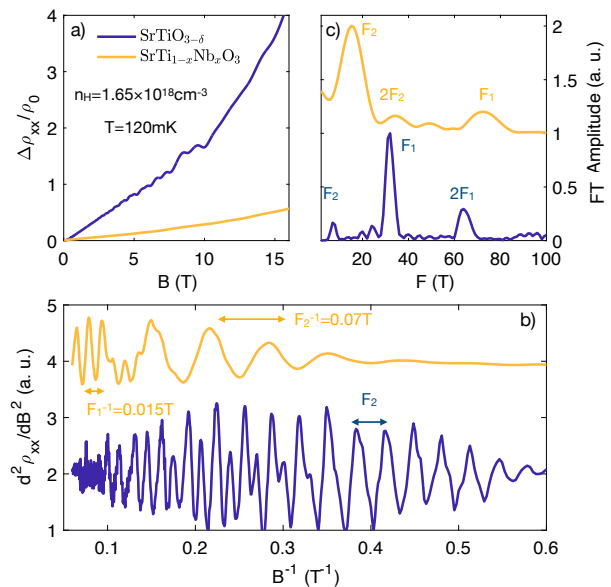


FIG. 2. **Distinct Fermi surfaces:** a) Magnetoresistance ($\frac{\Delta \rho_{xx}}{\rho_0}$) vs B in SrTi_{1-x}Nb_xO₃ (orange) and SrTiO_{3- δ} (blue) with the same Hall carrier density $n_H = 1.65 \times 10^{18} \text{cm}^{-3}$ at $T = 120$ mK. b) Traces of the quantum oscillations in $\frac{\partial^2 \rho_{xx}}{\partial B^2}$ as function of B^{-1} for both samples. c) Amplitude of the Fourier transform (FT) vs frequency (F) deduced from b). The amplitude was normalized by the peak value and shift for clarity. In both samples, two frequencies (and their harmonics) can be identified, respectively labelled F_1 and F_2 .

the supplement for more details about samples and data [35]).

Fig.1.b draws the superconducting phase diagram of SrTiO_{3- δ} and in SrTi_{1-x}Nb_xTiO₃ according to the available data reported by different groups [2, 22, 31]. The critical temperature does not evolve identically. The peak in T_c of the principal dome is higher in Nb-doped strontium titanate, while a lower superconducting dome is present for SrTiO_{3- δ} and absent in SrTi_{1-x}Nb_xO₃.

Evidence for superconductivity in this density range is limited to the detection of zero resistivity. The critical temperature of bulk probes of superconductivity, such as specific heat [36], thermal conductivity [36] and diamagnetism [37] is consistently lower than the temperature at which resistivity drops to zero. Given the strong variation of critical temperature with pressure or strain [18], this points to the survival of filamentary superconductivity with a higher critical temperature at specific locations like dislocations or domain boundaries. Nevertheless, oxygen-reduced samples display bulk superconductivity for a carrier density as low as $4.5 \times 10^{18} \text{cm}^{-3}$ [19, 22] and the Nb-substituted ones do not show any transition (resistive or else) at this concentration. Therefore, there is a genuine difference of the ground states, irrespective of the origin of filamentary superconductivity.

Let us now compare the normal state of these two di-

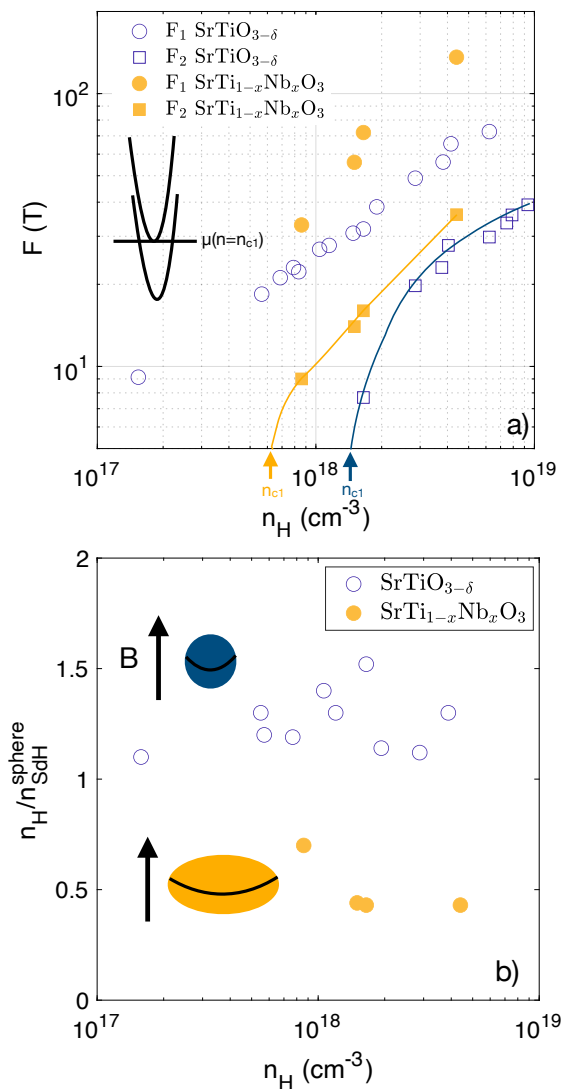


FIG. 3. **Doping evolution of the Fermi surface of $\text{SrTi}_{1-x}\text{Nb}_x\text{O}_3$ and $\text{SrTiO}_{3-\delta}$** : a) Frequencies of the quantum oscillations of the two sub-bands F_1 (circles) and F_2 (squares) *vs.* the Hall carrier density (n_H) in $\text{SrTi}_{1-x}\text{Nb}_x\text{O}_3$ and in $\text{SrTiO}_{3-\delta}$ [29]. b) Ratio of the Hall number with the carrier density deduced from quantum oscillations frequency assuming spherical sub-bands: $n_{\text{SdH}}^{\text{sphere}} = \frac{1}{3\pi^2} \left(\sqrt{\left(\frac{2eF_1}{h}\right)^2} + \sqrt{\left(\frac{2eF_2}{h}\right)^2} \right)$.

lute metals. Structurally, the distribution of oxygen vacancies is known to be less homogeneous than the distribution of Nb atoms [38]. However, in both cases, electrons belong to a single Fermi sea (and not to a plurality of puddles). Since the Bohr radius is as long as several hundreds of nanometer [39], disorder is averaged over a volume containing many dopants. In both oxygen-reduced and Nd-substituted strontium titanate, the carrier mean-free-path is much longer than the interdopant distance and quantum oscillations are visible at moderate (≈ 2 T) magnetic fields.

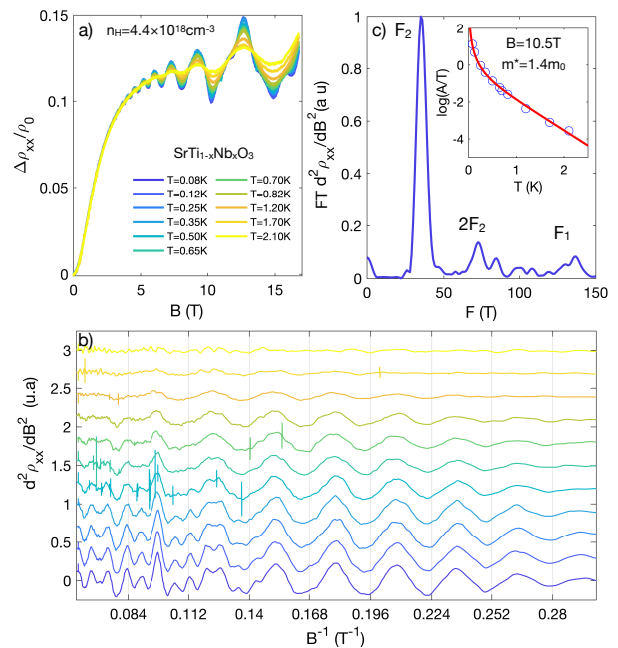


FIG. 4. **Quantum oscillations in $\text{SrTi}_{1-x}\text{Nb}_x\text{O}_3$ with $n_H = 4.4 \times 10^{18} \text{cm}^{-3}$** : a) $\frac{\Delta \rho_{xx}}{\rho_0}$ vs B at different temperatures from 80 mK to 2.1 K. b) $\frac{\partial^2 \rho_{xx}}{\partial B^2}$ as a function of B^{-1} displaying quantum oscillations. c) FT of the data at $T = 80$ mK. Inset: Temperature dependence of the amplitude of the oscillation at $B = 10.5$ T. The red line corresponds to a fit using the Lifshitz-Kosevich formula with $m^* = 1.4m_0$.

We carried out a careful examination of the structure of the Fermi surface by looking at the Shubnikov-de Haas effect in the two cases. Magnetoresistance ($\frac{\Delta \rho_{xx}}{\rho_0}$) at $T = 120$ mK and for $B \parallel [001]$ (See Fig.2a)) reveals a difference. Quantum oscillations are visible on top of a monotonic background in both. As seen in Fig.2b, however, despite the quasi-equality of their Hall carrier density, the second derivative of resistivity $\frac{\partial^2 \rho_{xx}}{\partial B^2}$ shows different patterns. Two main frequencies, labelled F_1 and F_2 can be resolved, in qualitative agreement with previous studies of quantum oscillations [5, 40, 41]. However, F_1 and F_2 are not identical in the two cases, implying a difference in the structure of the Fermi surface between superconducting $\text{SrTiO}_{3-\delta}$ and non-superconducting $\text{SrTi}_{1-x}\text{Nb}_x\text{TiO}_3$.

By studying three other Nb-doped thin-film samples with n_H ranging from $8.6 \times 10^{17} \text{cm}^{-3}$ to $4.4 \times 10^{18} \text{cm}^{-3}$ (see [35] for sample details), we found that the evolution of F_1 and F_2 in $\text{SrTi}_{1-x}\text{Nb}_x\text{O}_3$ and in SrTiO_{3-x} [29] are not identical (See Fig. 3.a). At a given Hall carrier density, both frequencies are larger in $\text{SrTi}_{1-x}\text{Nb}_x\text{O}_3$ compared to $\text{SrTiO}_{3-\delta}$ (See the supplement [35] for more details on the analysis).

In absence of an angle-dependent study, possible multiplicity of structural domains below 105 K is a source of complication. In multi-domain samples the orientation of magnetic field can be perpendicular or parallel to

the *c*-axis according to the orientation of domains. However, a simple procedure reveals a difference in Fermi surface sphericity in the two cases. Assuming that the two sub-bands are isotropic, the carrier density can be deduced from the frequencies of quantum oscillations: $n_{SdH}^{sphere} = \frac{1}{3\pi^2} (\sqrt{\frac{2eF_1}{h}} + \sqrt{\frac{2eF_2}{h}})$ and then compared to the Hall carrier density, n_H . Their ratio, $\frac{n_H}{n_{SdH}^{sphere}}$, is a measure of the deviation of the pockets from perfect spheres. Fig. 3.b compares the two cases at different doping levels. The ratio is ≈ 1.2 in $\text{SrTiO}_{3-\delta}$ and ≈ 0.5 in $\text{SrTi}_{1-x}\text{Nb}_x\text{O}_3$. Thus, the Fermi surface of Nb-doped samples is less spherical than the Fermi surface of $\text{SrTi}_{1-x}\text{Nb}_x\text{O}_3$. Moreover, as seen in Fig. 3.a, the threshold for filling the second band, i.e. the onset of the Lifshitz transition is also lower in the Nb-doped case.

We note that F_1 and F_2 of our Nb-doped samples are in good agreement with what has been found in La-doped samples [41]. This suggests that the Fermi surface in La-doped and in Nb-doped strontium titanate are similar. Interestingly, there is no report of a superconducting transition in single crystals [20] or thin films of $\text{Sr}_{1-x}\text{La}_x\text{TiO}_3$ [21] when the carrier density at very low ($\approx 10^{18} \text{ cm}^{-3}$) doping.

By studying the temperature dependence of the quantum oscillations and using the Lifshitz-Kosevitch formalism, we extracted the cyclotron mass of electrons. Fig. 4 shows the quantum oscillations and their temperature dependence in the sample with highest carrier concentration ($n_H = 4.4 \times 10^{18} \text{ cm}^{-3}$). The results of the analysis are shown in the upper panel of Fig. 4c). We find an effective mass of $m^* = 1.4 \pm 0.1m_0$ for the lower band, comparable to the value found previous studies of Nb-doped [40] (and La-doped [41]) strontium titanate. In contrast, the effective mass of the lower band in the oxygen-reduced case at this carrier density is $m^* = 1.8 m_0$ [5]. Thus, there is a small, but significant, difference in the magnitude of the effective mass [42].

Numerical emulation of a regime as dilute as the one explored experimentally requires unrealistically large supercells. Therefore, a quantitative and microscopic explanation of the observed difference is challenging. However, considerable insight can be gained from DFT calculations. To this end, we used the projected augmented wave pseudo-potential code VASP [43] to fully optimize the crystal structure, including the lattice parameters, in the $8 \times 8 \times 8$ supercell of 64 formula units, replacing one Ti by one Nb, or removing one O (see the supplement [35] for details). The unperturbed unit cell, as expected, optimizes into the $P4/m$ symmetry. The Nb case and, interestingly, the vacancy case both optimize into $P4/m$ with accuracy of 0.2 mÅ. On a structural level, there is already an interesting difference between the two cases. The energy gain between the tetragonal and quasicubic settings, which is 3.4 meV/formula in the undoped compound, becomes 4.7 meV for Nb substitution, and 0.9 meV for O vacancy. Strontium titanate goes through a cubic-to-tetragonal structural phase transition [44]. The transition temperature, which is $T_s \simeq 105 \text{ K}$

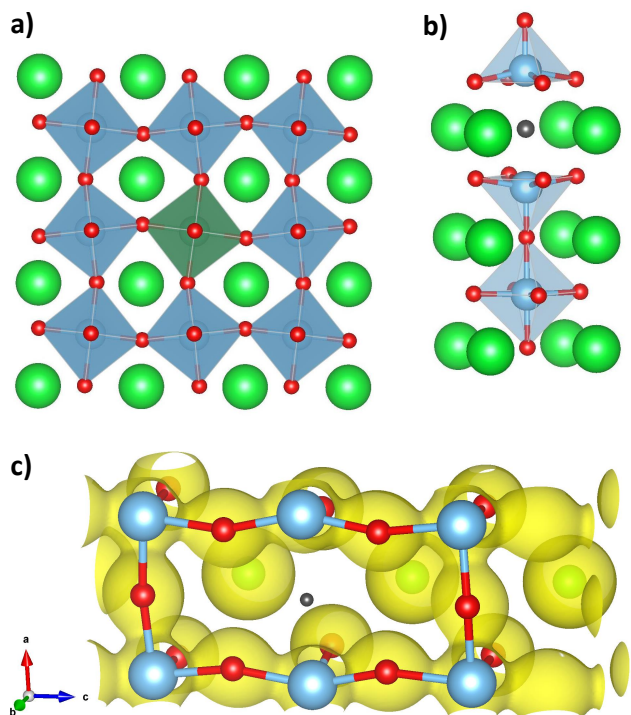


FIG. 5. **Effect of a Nb impurity (left, green octahedron) or an O vacancy (black ball) on the crystal structure and electron density.** The lower panel shows the electron charge distribution around the vacancy; here the red balls are O, the blue-grey ones Ti and Sr are green. The black ball indicates the approximate location of the vacancy. The (yellow) isosurfaces are drawn at the level of electron density of $0.05 \text{ e}/\text{Å}^3$.

for the pristine compound, increases by Nb substitution and decreases by oxygen deficiency [45, 46]. In a first approximation, T_s tracks this energy and therefore our calculations provide a qualitative account of the experimental observation.

The difference in the electronic structure (Fig. 6) is even more spectacular. Nb doping has little effect on the band dispersions, but the O vacancy dramatically modifies them. The main effect is the relative shift between the two lower (xz and yz) bands and the upper (xy) band. This can be understood by analyzing the change of the local crystal field. As Fig. 5 shows, Nb introduces no visible additional distortion, while the vacancy alters the local environment of the two neighboring Ti from octahedral to pyramidal, and leads to a visible relaxations of the eight closest oxygens.

Neglecting the small distortion of the octahedra, at the Γ point, which is the only one of interest, the hybridization of a Ti t_{2g} orbital with the four neighboring O atoms cancels out by symmetry (Fig. 7). However, if one apical oxygen is removed, the ligand field of the opposite one is uncompensated, so the corresponding band state is pushed up. In our case, this means that the xz and yz bands will be pushed up closer to the (unaffected) xy

band *at the Γ point* (but not at the Z point). Of course, given the delocalization of the doped electrons, the effect on the entire band is reduced compared to the actual change of the site-local crystal field, but it still rather large on the scale of interest (i.e., ~ 10 meV). Note that no extra electron density is calculated near the vacancy site (Fig. 7).

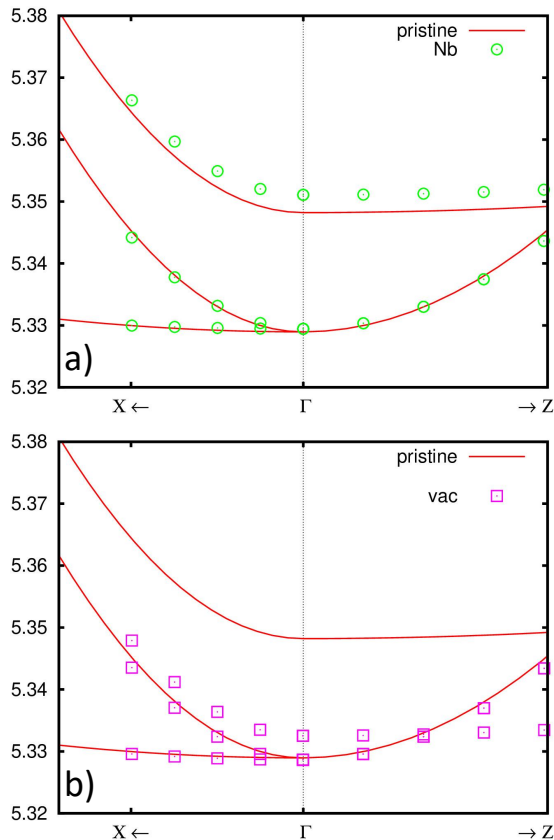


FIG. 6. **Non-relativistic band states in $\text{Sr}_{64}\text{Ti}_{63}\text{NbO}_{192}$ (a) and in $\text{Sr}_{64}\text{Ti}_{64}\text{O}_{191}$ (b)** In both cases, the structure was fully optimized within DFT. Note the dramatic shift of the upper band due to the change of crystallographic environment of two Ti atoms out of 64 from octahedral to pyramidal. The leftmost point, labelled as $X \leftarrow$, corresponds to 1/10 of the Γ -X distance, and the rightmost point, $\rightarrow Z$, to 1/10 of the Γ -Z.

Interestingly, the calculated threshold for the first Lifshitz transition in the pristine crystal [30] is $n_{c1} = 6.4 \times 10^{17} \text{cm}^{-3}$. This is in quantitative agreement what we find experimentally for $\text{SrTi}_{1-x}\text{Nb}_x\text{O}_3$ ($n_{c1} = 6.5 \pm 2 \times 10^{17} \text{cm}^{-3}$; Fig.4a), confirming that the rigid band approximation holds in this case (but not in $\text{SrTiO}_{3-\delta}$).

Thus, according to our experiments, Nb substitution and oxygen reduction generate different Fermi surface geometries and ground states and our calculations confirm a difference in the band dispersion between the two cases. Soft Transverse Optical (TO) phonons, suspected to play a key role in dilute superconductivity [23–27] may couple

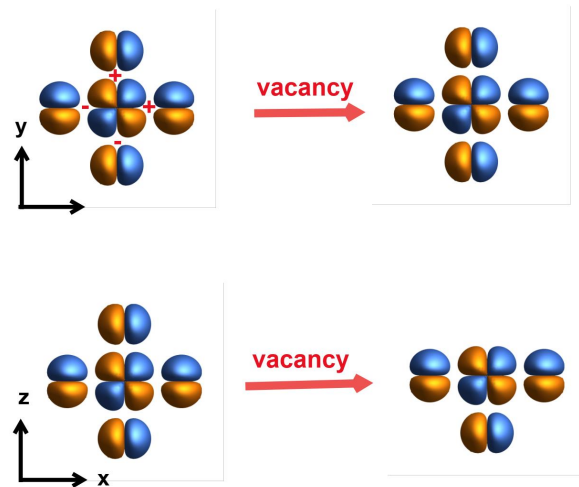


FIG. 7. **Effect of an O vacancy on the ligand crystal field** Relevant Ti d and O p wave functions for the wave vector \mathbf{k} corresponding to the Γ point, in the real space around a Ti site. In absence of O vacancy, the hybridization of all t_{2g} orbitals with the O states cancels out by symmetry. Introducing a vacancy does not change this for the xy orbital (top) but the cancellation is broken by the vacancy for the xz and yz (not shown) orbitals (bottom). As a consequence, in the momentum space, the corresponding bands at the Γ point shift upward.

more strongly to the electrons in this band than to the electrons in the regular conduction band. The dispersion of these TO phonons has been found to smoothly evolve with doping [7, 47]. Future studies may discriminate between the fingerprints of the two doping routes.

Dopant-dependent superconductivity has been reported in other cases. Beyond a critical threshold of Tl doping, $\text{Pb}_{1-x}\text{Tl}_x\text{Te}$ is a superconductor, but $\text{Pb}_{1-x}\text{Na}_x\text{Te}$ is non-superconducting [48, 49]. The difference has been tracked to the presence of Tl impurity states near the Fermi energy. Like the present case, a tiny concentration of extrinsic atoms is sufficient to modify the band structure of the stoichiometric host, documenting a breakdown of the rigid band approximation. Let us note that the concentration of dopants is two orders of magnitude lower in strontium titanate than in lead telluride. The experimental observation of dopant dependent superconductivity has motivated theoretical scenarios [50, 51], which may be relevant to our result. Nevertheless, large Hubbard correlations are unlikely to be large in the extreme dilute limit and Occam's razor [52] would favor scenarios which do not require them.

In summary, we found that doping strontium titanate by removing oxygen leads to a dilute metal different from the one obtained by substituting Ti with Nb. The two detected differences are the band dispersion and the presence and absence of a superconducting instability. The exceptionally dilute superconductivity is an instability in a band specifically sculpted by oxygen vacancies of stron-

tium titanate.

We thank Claude Ederer and Maria Gastiasoro for useful discussions. This work was supported by the Agence Nationale de la Recherche (ANR-18-CE92-0020-01; ANR-19-CE30-0014-04), by Jeunes Equipes de l'Institut de Physique du Collège de France and by a grant attributed by the Ile de France regional council. It

was funded in part by a QuantEmX grant from ICAM and the Gordon and Betty Moore Foundation through Grant GBMF9616 to KB. The work at SLAC/Stanford is supported by the U.S. Department of Energy, Office of Basic Energy Sciences, Division of Materials Sciences and Engineering, under Contract No. DE-AC02-76SF00515.

-
- [1] J. F. Schooley, W. R. Hosler, and M. L. Cohen, *Phys. Rev. Lett.* **12**, 474 (1964).
- [2] C. Collignon, X. Lin, C. W. Rischau, B. Fauqué, and K. Behnia, *Annual Review of Condensed Matter Physics* **10**, 25 (2019).
- [3] M. N. Gastiasoro, J. Ruhman, and R. M. Fernandes, *Annals of Physics* **417**, 168107 (2020).
- [4] G. M. Eliashberg, *Sov. Phys. - JETP* **11**, 696 (1960).
- [5] X. Lin, Z. Zhu, B. Fauqué, and K. Behnia, *Phys. Rev. X* **3**, 021002 (2013).
- [6] H. Yoon, A. G. Swartz, S. P. Harvey, H. Inoue, Y. Hikita, Y. Yu, S. B. Chung, S. Raghu, and H. Y. Hwang, *arXiv e-prints*, arXiv:2106.10802 (2021).
- [7] C. Collignon, P. Bourges, B. Fauqué, and K. Behnia, *Phys. Rev. X* **10**, 031025 (2020).
- [8] A. Kumar, V. I. Yudson, and D. L. Maslov, *Phys. Rev. Lett.* **126**, 076601 (2021).
- [9] K. G. Nazaryan and M. V. Feigel'man, *Phys. Rev. B* **104**, 115201 (2021).
- [10] C. Collignon, Y. Awashima, Ravi, X. Lin, C. W. Rischau, A. Acheche, B. Vignolle, C. Proust, Y. Fuseya, K. Behnia, and B. Fauqué, *Phys. Rev. Materials* **5**, 065002 (2021).
- [11] K. A. Müller and H. Burkard, *Phys. Rev. B* **19**, 3593 (1979).
- [12] V. Martelli, J. L. Jiménez, M. Continentino, E. Baggio-Saitovitch, and K. Behnia, *Phys. Rev. Lett.* **120**, 125901 (2018).
- [13] X. Li, B. Fauqué, Z. Zhu, and K. Behnia, *Phys. Rev. Lett.* **124**, 105901 (2020).
- [14] X. He, D. Bansal, B. Winn, S. Chi, L. Boatner, and O. Delaire, *Phys. Rev. Lett.* **124**, 145901 (2020).
- [15] B. Fauqué, P. Bourges, A. Subedi, K. Behnia, B. Baptiste, B. Rössli, T. Fennell, S. Raymond, and P. Steffens, *arXiv e-prints*, arXiv:2203.15495 (2022).
- [16] S. E. Rowley, L. J. Spalek, R. P. Smith, M. P. M. Dean, M. Itoh, J. F. Scott, G. G. Lonzarich, and S. S. Saxena, *Nature Physics* **10**, 367 (2014).
- [17] J. M. Edge, Y. Kedem, U. Aschauer, N. A. Spaldin, and A. V. Balatsky, *Phys. Rev. Lett.* **115**, 247002 (2015).
- [18] C. Enderlein, J. F. de Oliveira, D. A. Tompsett, E. B. Saitovitch, S. S. Saxena, G. G. Lonzarich, and S. E. Rowley, *Nature Communications* **11**, 4852 (2020).
- [19] C. W. Rischau, X. Lin, C. P. Grams, D. Finck, S. Harms, J. Engelmayer, T. Lorenz, Y. Gallais, B. Fauqué, J. Hemberger, and K. Behnia, *Nature Physics* **13**, 643 (2017).
- [20] Y. Tomioka, N. Shirakawa, K. Shibuya, and I. H. Inoue, *Nature Communications* **10**, 738 (2019).
- [21] K. Ahadi, L. Galletti, Y. Li, S. Salmani-Rezaie, W. Wu, and S. Stemmer, *Science Advances* **5**, eaaw0120 (2019), <https://www.science.org/doi/pdf/10.1126/sciadv.aaw0120>.
- [22] C. W. Rischau, D. Pulmannová, G. W. Scheerer, A. Stucky, E. Giannini, and D. van der Marel, *Phys. Rev. Research* **4**, 013019 (2022).
- [23] D. van der Marel, F. Barantani, and C. W. Rischau, *Phys. Rev. Research* **1**, 013003 (2019).
- [24] D. E. Kiselov and M. V. Feigel'man, *Phys. Rev. B* **104**, L220506 (2021).
- [25] P. A. Volkov, P. Chandra, and P. Coleman, *Nature Communications* **13**, 4599 (2022).
- [26] M. N. Gastiasoro, M. E. Temperini, P. Barone, and J. Lorenzana, *Phys. Rev. B* **105**, 224503 (2022).
- [27] Y. Yu, H. Y. Hwang, S. Raghu, and S. B. Chung, *npj Quantum Materials* **7**, 63 (2022).
- [28] K. L. Ngai, *Phys. Rev. Lett.* **32**, 215 (1974).
- [29] X. Lin, G. Bridoux, A. Gourgout, G. Seyfarth, S. Krämer, M. Nardone, B. Fauqué, and K. Behnia, *Phys. Rev. Lett.* **112**, 207002 (2014).
- [30] D. van der Marel, J. L. M. van Mechelen, and I. I. Mazin, *Phys. Rev. B* **84**, 205111 (2011).
- [31] Y. Tomioka, N. Shirakawa, and I. H. Inoue, *arXiv e-prints*, arXiv:2203.16208 (2022).
- [32] Z. Hou and K. Terakura, *Journal of the Physical Society of Japan* **79**, 114704 (2010), <https://doi.org/10.1143/JPSJ.79.114704>.
- [33] J. Souto-Casares, N. A. Spaldin, and C. Ederer, *Phys. Rev. Research* **3**, 023027 (2021).
- [34] Y. Kozuka, Y. Hikita, C. Bell, and H. Y. Hwang, *Applied Physics Letters* **97**, 012107 (2010), <https://doi.org/10.1063/1.3457994>.
- [35] See Supplemental Material for more details and additional data regarding the samples and the methods.
- [36] X. Lin, A. Gourgout, G. Bridoux, F. m. c. Jomard, A. Pourret, B. Fauqué, D. Aoki, and K. Behnia, *Phys. Rev. B* **90**, 140508 (2014).
- [37] C. Collignon, B. Fauqué, A. Cavanna, U. Gennser, D. Maily, and K. Behnia, *Phys. Rev. B* **96**, 224506 (2017).
- [38] K. Szot, W. Speier, R. Carius, U. Zastrow, and W. Beyer, *Phys. Rev. Lett.* **88**, 075508 (2002).
- [39] K. Behnia, *Journal of Physics: Condensed Matter* **27**, 375501 (2015).
- [40] H. Uwe, R. Yoshizaki, T. Sakudo, A. Izumi, and T. Uzunaki, *Japanese Journal of Applied Physics* **24**, 335 (1985).
- [41] S. J. Allen, B. Jalan, S. Lee, D. G. Ouellette, G. Khalsa, J. Jaroszynski, S. Stemmer, and A. H. MacDonald, *Phys. Rev. B* **88**, 045114 (2013).
- [42] The lower band is non-parabolic [30], and therefore, the effective mass is expected to increase with increasing carrier density. Experimentally, m^* in the oxygen-doped samples becomes $\approx 3.5 m_0$ at $n_H = 3 \times 10^{19} \text{ cm}^{-3}$ [29].
- [43] G. Kresse and J. Hafner, *Phys. Rev. B* **47**, 558 (1993).

- [44] F. W. Lytle, *Journal of Applied Physics* **35**, 2212 (1964), <https://doi.org/10.1063/1.1702820>.
- [45] D. Bäuerle and W. Rehwald, *Solid State Communications* **27**, 1343 (1978).
- [46] Q. Tao, B. Loret, B. Xu, X. Yang, C. W. Rischau, X. Lin, B. Fauqué, M. J. Verstraete, and K. Behnia, *Phys. Rev. B* **94**, 035111 (2016).
- [47] W. Rehwald, *Solid State Communications* **8**, 1483 (1970).
- [48] Y. Matsushita, H. Bluhm, T. H. Geballe, and I. R. Fisher, *Phys. Rev. Lett.* **94**, 157002 (2005).
- [49] P. Giraldo-Gallo, P. Walmsley, B. Sangiorgio, S. C. Riggs, R. D. McDonald, L. Buchauer, B. Fauqué, C. Liu, N. A. Spaldin, A. Kaminski, K. Behnia, and I. R. Fisher, *Phys. Rev. Lett.* **121**, 207001 (2018).
- [50] M. Dzero and J. Schmalian, *Phys. Rev. Lett.* **94**, 157003 (2005).
- [51] S. A. Kivelson, *Journal of Superconductivity and Novel Magnetism* **33**, 5 (2020).
- [52] I. Mazin, *Nature Physics* **18**, 367 (2022).
- [53] H. Inoue, H. Yoon, T. A. Merz, A. G. Swartz, S. S. Hong, Y. Hikita, and H. Y. Hwang, *Applied Physics Letters* **114**, 231605 (2019), <https://doi.org/10.1063/1.5090269>.
- [54] A. Spinelli, M. A. Torija, C. Liu, C. Jan, and C. Leighton, *Phys. Rev. B* **81**, 155110 (2010).
- [55] J. P. Perdew, K. Burke, and M. Ernzerhof, *Phys. Rev. Lett.* **77**, 3865 (1996).
- [56] K. Momma and F. Izumi, *Journal of Applied Crystallography* **44**, 1272 (2011).

Supplementary Material

S1. Samples

The present study compared the fermiology and the superconducting transition in thin films of $\text{SrTi}_{1-x}\text{Nb}_x\text{O}_3$ and in single crystals of $\text{SrTiO}_{3-\delta}$.

Nb-doped films were synthesized on SrTiO_3 (001) substrate in pulsed laser deposition. A cap and buffer layer were used to prevent significant surface depletion in the doped layer [53]. The growth recipes were described previously, resulting in a similar carrier density and mobility of films to those of bulk crystals [34]. Particularly for S4, we repetitively switched two targets of 0.02 at.% of Nb and undoped to synthesize the lower carrier density than the nominal density of the Nb target. In order to keep the uniform dopant distribution avoiding the effects of superlattices, the pulse number for a single period (6 pulses for Nb-doped, 6 pulsed for undoped) was intentionally set to be lower than the pulse number needed for growing one unit cell (16 pulses).

Oxygen-deficient SrTiO_3 samples were obtained by annealing commercially bought substrates in an oven in a temperature range of 700°C to 1000°C under vacuum ($< 10^{-6}$ mbar) [5, 54].

Sample	μ_H ($\text{V}\cdot\text{cm}^{-2}\cdot\text{s}^{-1}$)	n_H (cm^{-3})	F_1 (T)	F_2 (T)	dopant	thickness (nm)	Undoped cap layer (nm)
S_1	4100	$4.4\text{e}18$	36	137	0.04 at.% Nb	892	119
S_2	3162	$1.65\text{e}18$	16	72	0.02 at.% Nb	617	102
S_3	1365	$1.5\text{e}18$	14	58	0.02 at.% Nb	895	90
S_4	9084	$8.6\text{e}17$	9	33	0.02 at.% Nb + undoped	748	100

TABLE S1. Properties of $\text{SrTi}_{1-x}\text{Nb}_x\text{O}_3$ thin film samples. The Hall mobilities are given at 2 K.

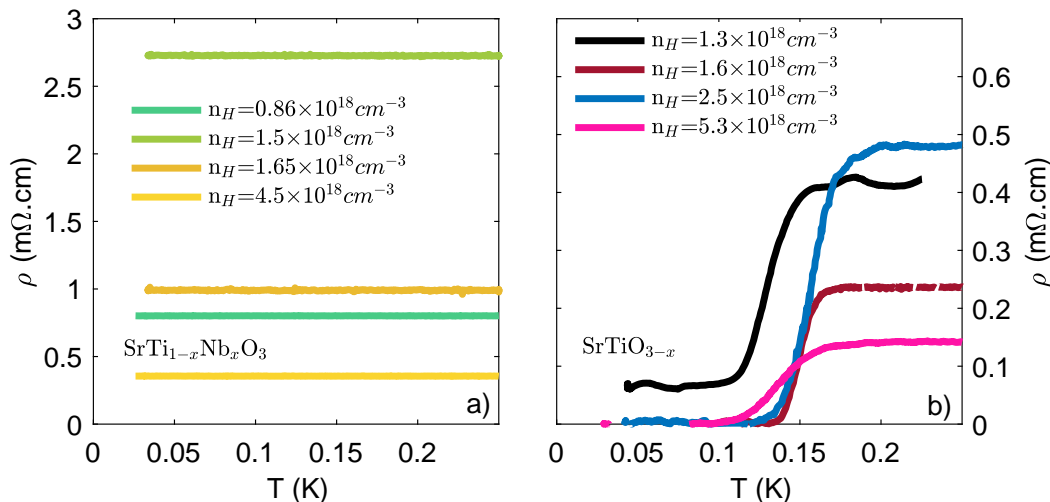


FIG. S1. Low temperature dependence of the resistivity (ρ) in $\text{SrTi}_{1-x}\text{Nb}_x\text{O}_3$ (a) and in $\text{SrTiO}_{3-\delta}$ (b). Hall carrier densities range from 10^{18}cm^{-3} to $5 \times 10^{18} \text{cm}^{-3}$. $\text{SrTiO}_{3-\delta}$ is a superconductor and $\text{SrTi}_{1-x}\text{Nb}_x\text{O}_3$ is not.

S2. Reproducibility

Tab.S1 lists the electronic properties of the four Nb thin film samples studied. At low temperature, none of these samples display a superconducting transition. This is in sharp contrast with oxygen-reduced samples of similar Hall carrier density (see Fig.S1), as reported by previous studies [22, 31, 37].

As discussed in the main text, this difference is concomitant with a difference in the Fermi surface geometries. Fig. S2 shows the trace of the quantum oscillations and its Fourier Transform for the four Nb-doped samples. In all

samples, two main frequencies, labelled F_1 and F_2 , are detected as well as their harmonics. The evolution of F_1 and F_2 with doping is shown in Fig.3 of the main manuscript.

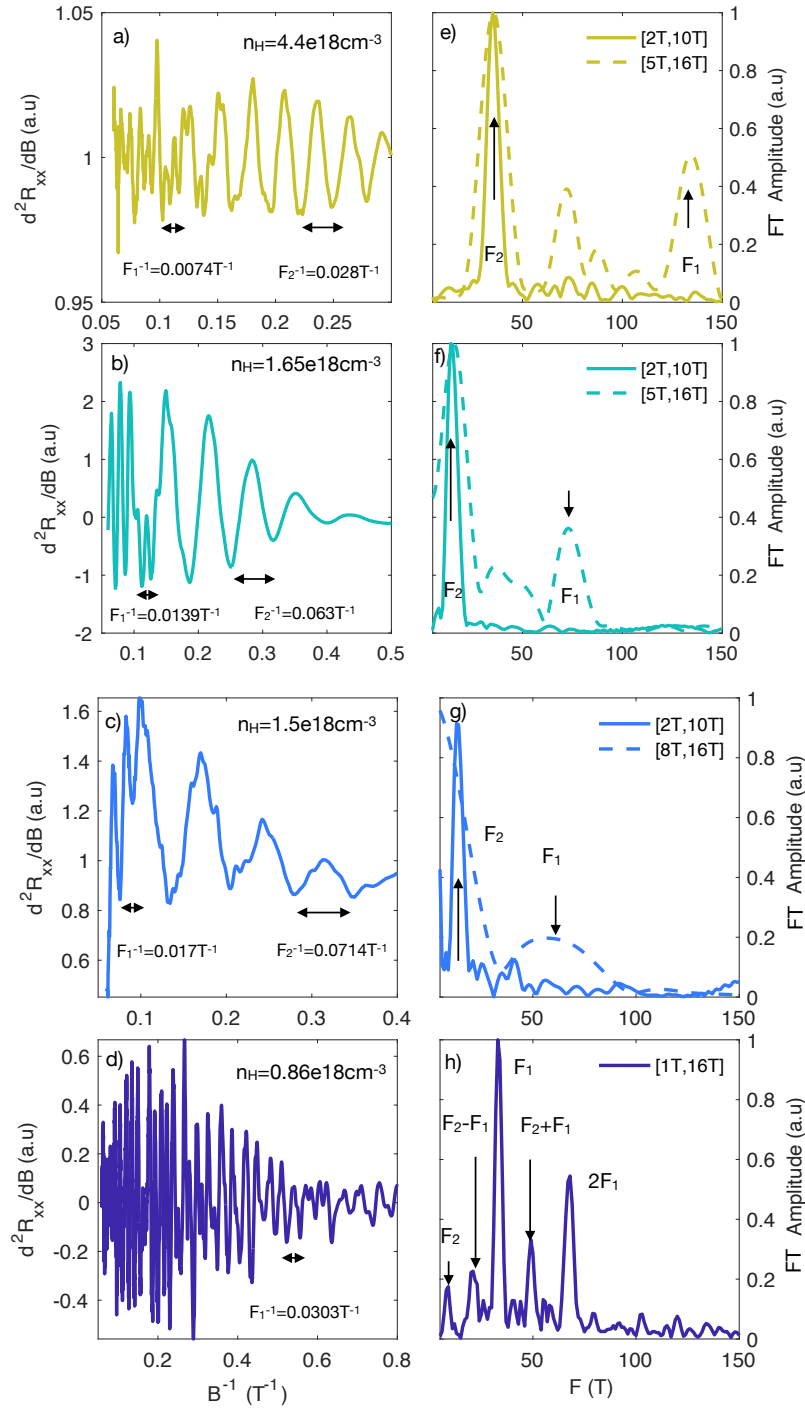


FIG. S2. a)-d) Quantum oscillations of $\frac{\partial^2 R_{xx}}{\partial B^2}$ in the four $SrTi_{1-x}Nb_xO_3$ samples studied at low temperature. e-h) Normalised amplitudes of the Fourier transform deduced from a)-d). In three cases, two different field windows were used for performing Fourier transform to highlight the emergence of a second frequency at high magnetic field.

As one can see, in all these samples there is more than one frequency. The higher frequency, which corresponds to the lower filled band or the outer Fermi surface pocket, is only detectable at higher fields and therefore its detection by a Fourier transform requires to restrict the analysis to a higher field window.

S3. Calculations

We used the Projector Augmented Wave method in conjunction with the Generalized Gradient Correction to the exchange-correlation potential [55], as implemented in the VASP package [43]. We used an 8x8x8 quasi-cubic supercell to emulate either defect. Gaussian smearing with $\sigma = 20$ meV was used, and the k -point mesh was 2x2x2. The plane-wave cutoff was 400 eV. Note that full structural optimization was performed, as opposed to Ref. [30], where the experimental low-temperature structure was used (the latter approach is more accurate, but not possible for the doped cases).

The resulting structures can be downloaded as Supplementary files Sr64NbTi63O192.cif and Sr64Ti64O191.cif. Visualization used in Fig. 5 in the main text was generated using the VESTA program [56].